Solid State Probe Design

F. David Doty

Doty Scientific Inc., Columbia, SC, USA

1 INTRODUCTION

Obtaining detailed structural information from NMR of solid samples is more complex than for liquids because of the absence of molecular tumbling in solids to average line-broadening interactions; hence, much greater probe bandwidths are required.[1–4] The wideline probe usually has spectral excitation bandwidth greater than 80 kHz (i.e., able to generate 90° pulses less than 3 μs). To do this, it normally must withstand peak rf voltages in excess of 3 kV. Often wideline probes are double-tuned (DT) to permit cross polarization (CP) and high-power decoupling for increased sensitivity and resolution. If $\pi/2$ pulse lengths below 2 μs can be generated, multiple pulse line-narrowing techniques may be used to remove dipolar broadening,[3] but this is generally possible only in single resonance probes where low inductance coils can be used effectively.

The most common solids probe is the cross polarization/magic angle spinning (CP MAS) probe, which adds high-speed sample spinning at the magic angle to the other capabilities of the DT wideline probe for effective averaging of the chemical shift anisotropy (and perhaps dipolar broadening at very high speeds), thereby greatly improving resolution for spin-$\frac{1}{2}$ nuclei.[5] Single resonance MAS probes can generate the short pulses needed for the combined rotation and multiple pulse spectroscopy (CRAMPS) line-narrowing technique for ^{1}H or ^{19}F. Large volume MAS rotors can achieve the rotational spin rate stability needed for slow MAS, where pulses are applied at precise rotor orientations to average out the anisotropic chemical shift broadening as with high-speed MAS, although sensitivity may be reduced. Commercially available extended variable temperature (X-VT) CP MAS probes permit experiments from 35 K to 650 °C.

When sufficiently large single crystals of the sample can be grown, high-resolution spectra and the chemical shift tensor can be obtained using a single crystal probe,[6] which is similar to a wideline probe but includes a goniometer and crystal orientation mechanism for rotating the sample about three perpendicular axes.

Quadrupolar interactions require more complex motions for effective averaging.[7] The dynamic angle spinning (DAS) probe allows the spinning axis to be changed rapidly while spinning the sample at high speeds. In another approach, known as double rotation (DOR), the sample is placed in a small spinner inside a larger spinner and spun about two intersecting axes simultaneously.

The short T_2 values (and often long T_1 values) in solids make sensitivity much lower than in liquids, and the requirement for high-power decoupling requires attention to efficiency at the proton frequency. In liquids probes, it is the sample coil that is most critical. For solids, it is the capacitors.

2 HIGH-POWER CAPACITORS

The special requirements of capacitors for NMR probes include the following: ultra-low magnetic susceptibility, high Q, high voltage, high current, ultra-low piezoelectric effects, and dielectrics devoid of unwanted NMR background signals. Losses in rf capacitors at a given frequency may be indicated by a capacitor quality factor Q_c, an effective series resistance [ESR = $(\omega C Q_c)^{-1}$], a loss tangent ($\tan\delta \cong \pi/Q_c$), or a loss factor, $k_d \tan\delta$, where k_d is the dielectric constant (relative permittivity). Direct current losses may be specified by a leakage resistance, but this usually has no relationship to R_P (the effective parallel resistance of a tuned circuit) above 1 MHz. Table 1 lists typical permittivity and loss properties of dielectrics frequently encountered in NMR probes.[8–12]

Solids probes are usually designed for peak voltages of 2.5–4 kV, compared with ~1 kV for most liquids probes. Voltage breakdown strengths often tabulated for dielectrics are best ignored unless two important parameters are also specified: test material thickness and frequency. The frequency dependence is

Table 1 Dielectric Properties

Dielectric	k_d	$\tan\delta$[a]
Teflon, PE, PP	2.0–2.2	0.0002+
Kel-F	2.5	0.001
PMMA	2.8	0.03
PEK	3.4	0.003
Vespel	3.5	0.004
Epoxy	3.6	0.03
Quartz	3.8	0.0001
Macor	5.5	0.005
Porcelains	5–8	0.0002+
Si_3N_4[b]	8	0.001+
MgO	9.65	0.0005
Al_2O_3 (sapphire)	9.9	0.0002
PSZ (ZrO_2–MgO)	22	0.005+
BaO	34	0.001
COG	65–95	0.001
TiO_2	90	0.001
$SrTiO_3$	330	0.002+

[a]Loss tangent is approximate at 300 K, 30 MHz, and increases with temperature and frequency, especially in plastics and high-k dielectrics.

[b]High purity, high density, with minor Y–Al–Mg–O glass phase.

For References see p. 4484

Table 2 Typical Dielectric Breakdown Voltages

Thickness (mm)	V_B, k_d>30 (V)	V_B, k_d<10 (V)
0.1	500	1000
0.5	1200	2200
3.0	3000	5400

not easily characterized, but dc ratings of rf capacitors are typically four times the short-pulse rf ratings at 100 MHz. For very short pulses where heating is not much of a factor, the voltage rating at 10 MHz is typically only twice that at 500 MHz, but with long pulses the voltage derates at least as the $\frac{3}{2}$ power of the frequency above a cutoff that is a function of Q_c/C. Table 2 shows typical rf breakdown voltages, V_B, for several thicknesses of low-k and high-k dielectrics at 30 MHz. Above 50–100 V, V_B is a square root function of thickness and shows relatively little variation within the two classes of rf dielectrics listed.[11] Dry air has an ionization V_B comparable to that of high-k dielectrics, but arc voltage in monatomic gases (He, Ne, Ar) is less by a factor of at least five (more for large gaps) because of the absence of low-energy rotational and vibrational relaxation modes.[13] The additional rotational modes in polyatomic gases usually increase the breakdown voltage, except in the case of ionic gases such as H_2O.

2.1 Ceramic Capacitors

The standard COG (ceramic oxide glass) rf capacitor specification (formerly type NPO) requires a temperature coefficient of less than ±30 ppm and $\tan\delta$ below 0.001 for the range −55 °C to 125 °C. For moderate-power applications up to 300 MHz, the COG formulation usually consists of fine-grained baria–neodymia–titania systems or magnesium titanate prefired with 6 mol% calcium titanate, but they are also made from mixtures of neodymium carbonate, titania, and barium titanate. A two-stage firing is generally required for multilayer capacitors so that the final firing temperature can be kept below 1150 °C to allow the use of Pd–Ag electrodes. The ceramic precursors are prefired at a high temperature, then reground and mixed with a powdered glass binder with matched thermal expansion such as 36% CdO, 23% Bi_2O_3, 25% PbO, 5% ZnO, 5% B_2O_3, 5% SiO_2, 1% Al_2O_3.[9] Alternate layers of ceramic/glass and metallization slurry are built up by a screening or spraying process.

Porcelains (magnesium–aluminum–silicates) are often used in the UHF range for high-power capacitors below 15 pF. Corning Pyroceram 9606 consists mostly of cordierite ($2MgO–2Al_2O_3–5SiO_2$), with lesser amounts of cristobalite and various magnesium titanates. Its low thermal expansion can cause problems with the metallization. Forsterite ($2MgO\cdot SiO_2$) is electrically almost as good as Pyroceram, easier to produce, and easy to metallize, but has poor thermal shock resistance.

UHF high-power capacitors above 30 pF are usually based on strontium titanate, which is not piezoelectric but may contain piezoelectric barium titanate impurities. High-power rf capacitors are often coated with a sealing glass such as $2PbO\cdot SiO_2$ (550 °C) to keep out moisture,[8] as it facilitates silver migration in the presence of an electric field.

The magnetic properties of ceramic capacitors are unpredictable, as most ceramics are slightly diamagnetic (bismuth compounds are very diamagnetic), palladium is extremely paramagnetic, and ferromagnetic nickel barriers are sometimes used in the terminations. A number of manufacturers are by now quite familiar with the stringent requirements of NMR/MRI capacitors and offer 'nonmagnetic' chip capacitors with 500–1000 V rating (a 2.5–3 mm cube), but it is always necessary to screen them for magnetism using a small magnet (a 2-mm cube of high-energy neodymium–boron–iron) suspended from a string. Also, nearly 1% of new capacitors may be noisy in a double resonance circuit as a result of microgaps between the electrodes or terminations and the dielectric.[14] Premature breakdown may be initiated by surface tracking and moisture in solder rosin.

At least four manufacturers (JFD, ATC, Murata Erie, and Tansitor Electronics) offer 3-kV multilayer ceramic rf capacitors in roughly a 3.5 × 10 × 11 mm^3 package. The JFD capacitors have generally been found to have the highest Q, but the difference is often not important. Some of the best NMR ceramic capacitors (when available, but once discontinued) are the 2-kV UV10 and UV17 series (3.3 × 6 × 8 mm^3) by Murata Erie, as they have very low magnetic susceptibilities and a 2-kV rating in a small package. Moreover, for typical circuit values (reactance above 100 Ω), Q_c is usually greater than 3000 for capacitance below 150 pF at frequencies at least up to 50 MHz, and Q_c is usually greater than 1000 up to 500 MHz.

2.2 Piezoelectric Acoustic Ringing

While acoustic ringing is seldom a problem in liquids probes because of the longer T_2s and the effectiveness of the Patt acoustic suppression sequence,[15] piezoelectric-induced acoustic ringing[16] of capacitors can obscure signals in solids probes requiring short recovery times. Subjecting a capacitor with ferroelectric impurities to a dc electric field in excess of 1 $kV\,mm^{-1}$, as may occur in a voltage withstanding test or from asymmetric rf breakdown, causes domain alignment and imparts a net crystallographic piezoelectric orientation to the ceramic. The ferroelectric is said be 'poled', and may exhibit acoustic ringing. The polarization of ferroelectrics can be annealed out by heating above the Curie temperature (130 °C for $BaTiO_3$; 180–300 °C for lead–magnesium–niobates), but they can easily become poled again.

Grain size is usually under 4 μm for rf power COG capacitors in the 10–30 pF range, in which case Rayleigh scattering will normally keep acoustic decay times under a few μs above 30 MHz. However, grain size may exceed 100 μm in high-voltage (HV) capacitors above 150 pF and occasionally in low-valued capacitors, resulting in reduced acoustic absorption and acoustic decay times greater than 10 μs at frequencies as high as 45 MHz. On the other hand, acoustic ringing in bulk metals from the Lorentz interaction is seldom a problem above 15 MHz.[17]

2.3 Variable Capacitors

The double rotation (DOR) probe shown in Figure 1 illustrates the use of three common types of variable capacitors (air, quartz, and pressurized gas) and 3-kV ceramic chip

For list of General Abbreviations see end-papers

capacitors (attached to the left of the quartz variable near the center of the photo). The Johanson 5000-series nonmagnetic, air-dielectric, trimmer capacitor (one is mounted on the upper circuit board near the center of Figure 1, just to the right of the central support post) is typical of that used in most liquids NMR probes and the high-frequency (HF) channel in solids probes with capacitive voltage division. It consists of an alumina ceramic housing supporting several concentric, silver plated brass cylinders at the 'hot' end; a precision screw mechanism adjusts a similar intermeshing arrangement at the mount end. The minimum radial air gap is under 0.1 mm, and breakdown occurs at 500–700 V when new. With use, alignment deteriorates, and the voltage rating decreases. Care must be taken to avoid dissolving the internal lubricants (which are essential for an acceptable lifetime) with cleaning solvents. The capacitors may be sealed, but this is inconvenient; hence, their voltage rating also decreases with altitude and humidity or high concentrations of monatomic gases. These variable capacitors are manufactured using 300 °C Pb–Ag solder between the alumina and brass body parts, and they tolerate repeated overvoltages.

Also shown in Figure 1 (near the center, on top of a gas variable capacitor, just left of the central support post) is the JMC 7584, quartz-dielectric, 0.8–10 pF, variable capacitor. Its 2.5-kV rf capability allows five-times the tuning range of the above air variables, as tuning range is generally proportional to $(CV^2)^{\frac{1}{2}}$. Defective silver plating on the piston or sleeve has occasionally been found to produce noise at lower voltages in double resonance circuits.[14] Impurities in the brass base and piston of the JMC capacitor are not controlled as carefully as in a similar capacitor by Voltronics, but the JMC capacitor is more robust which simplifies certain capacitive voltage division arrangements,[18] and the magnetism is acceptable unless it must be very close to the sample. These capacitors have been used successfully up to 400 MHz. They may lock up at high temperatures from the piston expanding or at low temperatures from the lubricants freezing.

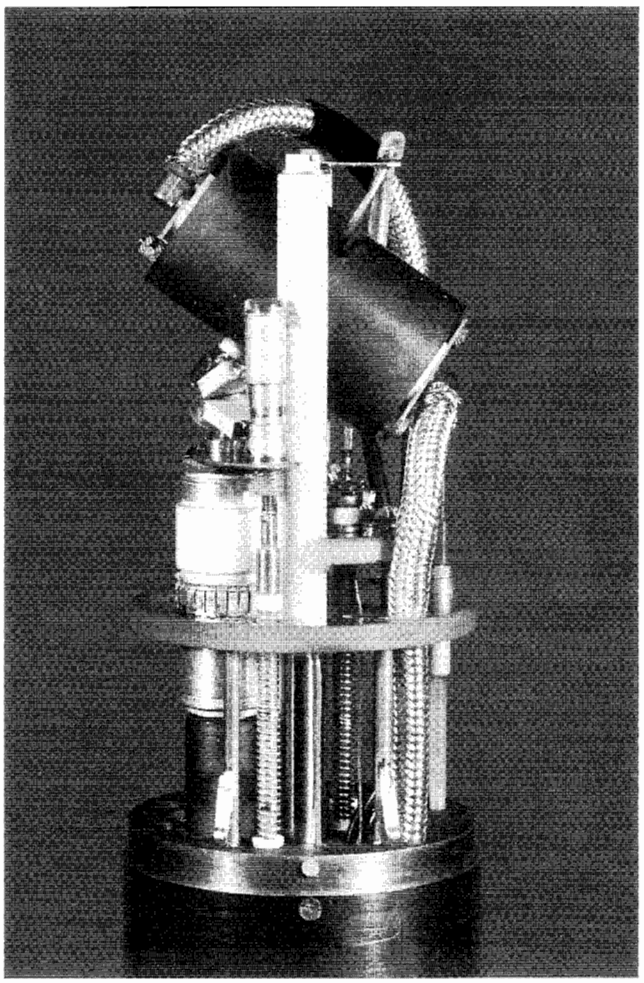

Figure 1 DOR WB probe (Doty Scientific, Inc.)

The single component most synonymous with solids NMR probes is the Jennings CHV1N-45 gas variable capacitor—the 22-mm diameter ceramic cylinder on the left side of the main circuit board in Figure 1. It is pressurized with about six atmospheres of CO_2 and SO_2 in its minimum capacitance position and may be adjusted from 1.5 pF to 45 pF using a pushrod mechanism. It has a peak breakdown voltage V_B of about 3.5 kV near the low end of its range (~10 pF) but V_B increases to about 5 kV near the high end as the gas becomes more compressed. The ceramic-to-metal seals are slightly magnetic, but this is seldom a problem as they are normally more than 20 mm from the sample. These variables have been used successfully for tuning purposes up to 220 MHz. With proper layout, they are usable on the low-frequency (LF) channels of multituned circuits with 500 MHz HF. These capacitors tolerate repeated overvoltages and are usable from −20 °C to 100 °C. If the external mechanical stop is not set properly, they may be easily damaged by pushing the adjustment rod beyond the specified limit.

Teflon variables with very low magnetism are available from Polyflon and Voltronics in a variety of sizes and ratings similar to the three described above, but Teflon does not tolerate the brief, inadvertent overvoltages which are unavoidable in most laboratories.

3 SAMPLE COILS FOR SOLIDS

Almost all solids probes use solenoidal rf coils for higher filling factor and Q than saddle coils. Standard oxygen-free, high-conductivity (OFHC) electronic-grade copper wire (C10100, 99.99%) has acceptably low iron content (less than 25 ppm, typically 4 ppm) for most solids coils at high fields. Optimum space between wires is half the wire diameter[19] or perhaps a little less. An enamel coating does not usually cause a background problem with carbon experiments, but it should be removed using warm sulfuric acid if proton experiments are planned.

High-Q circuits are usually preferred—except perhaps for wideline. Coil length-to-diameter ratio is not critical, but values between 1.0 and 1.4 (depending on available wire sizes) are usually best, except for MAS. Larger ratios (1.4–3.0) give better S/N for MAS (more sample for a given speed and lower dielectric losses), but some manufacturers use short coils to achieve shorter pulse lengths and higher decoupling fields. Coil forms help stabilize tuning but reduce both filling factor and maximum voltage before the onset of arcing. If used, they

For References see p. 4484

should be of low-permittivity dielectrics for minimal electric field gradients and arcing.

Special or custom wire may be obtained from MWS Wire Industries, Westlake Village, CA. Gold flash (0.3-μm plating) is often applied to prevent copper sulfates and chlorides (which have a large positive susceptibility due to antiferromagnetism) from forming on the wire surface, but it is critical to specify that the common practice of first applying a nickel strike (to

Table 3 Properties of NMR Probe Materials at 300 K

(a) Conductors

Material	Density	Young's modulus	Poisson ratio	Yield strength	Electrical conductivity	Thermal conductivity	Thermal expansion	Specific heat	Magnetic susceptibility
Symbol	d	E	r	S	σ	k_T	b_T	C_p	χ_v
Units	$kg\,m^{-3}$	GPa		MPa	$(MWm)^{-1}$	$W\,mK^{-1}$	$10^6\,K^{-1}$	$J\,(kg\,K)^{-1}$	10^{-6}
Aluminum	2700	69	0.33	30	36.6	230	22	900	21
Copper	8950	122	0.34	150	58.0	400	16.5	490	−9.8
Gold	19 300	78	0.42	20	44.0	315	14.2	128	−34
Hafnium	13 090	110	0.34	300	2.9	22	5.9	145	69
Iridium	22 500	440	0.27	1200	19.8	147	6.8	130	38
Molybdenum	10 200	320	0.3	300	18.1	138	5.2	276	120
Palladium	12 020	115	0.38	250	9.3	76	11.8	245	840
Rhodium	12 440	330	0.29	800	20.9	150	8.3	247	168
Silver	10 500	78	0.38	100	61.4	428	19	235	−24
Tungsten	19 250	410	0.28	1000	18.4	173	3.8	133	80
Zirconium[a]	6506	99	0.35	200	2.3	21	5.85	295	160
Al-6061T6[b]	2700	69	0.33	214	25	180	23.6	896	20
H. C-22[c]	8690	206	0.3	400	0.9	10	12.4	414	650
J-bronze[d]	8780	115	0.34	200	23.5	173	18.6	380	−10
P-bronze[e]	8860	110	0.35	200	11.5	84	17.8	380	−9.2
60/40PbSn	9700	30	0.4	40	6.3	45	24	176	~5
SS304[f]	8000	193	0.31	300	1.4	16	17	500	~3000

(b) Insulators

Material	Density	Young's modulus	Poisson ratio	Yield strength	Dielectric constant	Thermal conductivity	Thermal expansion	Specific heat	Magnetic susceptibility
Symbol	d	E	r	S	k_d	k_T	b_T	C_p	χ_v
Units	$kg\,m^{-3}$	GPa		MPa	$(M\Omega m)^{-1}$	$W\,mK^{-1}$	$10^6\,K^{-1}$	$J\,(kg\,K)^{-1}$	10^{-6}
99.5Al_2O_3	3950	390	0.22	240	9.9	35	8	780	−18
A-JGN3030[g]	1560	10	0.35	130	3.7	0.3	~35	960	−5
HIPd-Si_3N_4[h]	3250	310	0.26	710	7	25	3.2	740	−20
Kel-f	2100	1.3	~0.45	20	2.5	0.21	60	800	−10.6
Macor[i]	2520	64	0.28	80	5.9	1.7	9	750	~−15
99.5% MgO	3400	250	0.2	100	9.6	20	13.5	955	
PEK	1300	3.8	~0.4	70	3.3	0.24	54	1500	~−8
PSZ[j]	5700	200	0.25	500	23	3	9.5	490	−8
Pyrex-7070	2500	70	0.2	60	4.0	1.3	3.3	800	−11
Quartz[k]	2250	74	0.16	50	3.8	1.4	0.5	700	−16
Silica foam[l]	770	~20	–	~5	~1.5	~0.1	0.5	700	−3.5
Teflon	2200	0.4	~0.45	12	2–2.2	0.25	120	750	−9.8
Vespel[m]	1430	3.1	0.41	86	3.5	0.33	54	1130	−9
Water	997	0	–	0	80	0.6	–	4182	−9.06

Note: Volume susceptibility χ_v in SI is related to cgs molar susceptibility χ_m by: $\chi_v = 4\pi d\chi_m/(M.wt.)$.
[a]Commercially pure zirconium, grade 702: 96Zr, 3Hf, 0.1Cr, 0.1Fe.
[b]97Al, 1Mg, 0.6Si, 0.4Fe.
[c]Haynes C-22: 60Ni, 22Cr, 13Mo, 5W + Co.
[d]C22600: 88Cu, 12Zn, 0.005Fe.
[e]C51000: 95Cu, 5Sn, 0.1Fe.
[f]68Fe, 19Cr, 9Ni, 2Mn, 1Si.
[g]Aurum PI resin, 30% glass fiber.
[h]98Si_3N_4, 2Y_2O_3, HIPd.
[i]Al–B–Si–Mg–F ceramic glass, Corning.
[j]94ZrO_2, 3HfO_2, 3MgO.
[k]Fused silica, electronic grade.
[l]Fused silica foam, industrial grade.
[m]Dupont polyimide SP-1.

For list of General Abbreviations see end-papers

minimize diffusion into the copper) be omitted or the wire will be very magnetic. The gold flash degrades the Q by about 1%. Silver plating does not improve Q (because of unavoidable defects) and does not provide the same degree of protection against corrosion—even when the plating thickness is increased to 3 μm. Silver and its compounds are quite diamagnetic but often contain paramagnetic impurities.

High-purity copper coils for high resolution are often plated with the proper thickness of iridium or rhodium to cancel the diamagnetism of copper.[20] Palladium can also be used for this purpose if it is plated only on the side that will be the external surface of the coil (where there is little current flow) so that the Q is not spoiled. Table 3 lists various properties, including volumetric magnetic susceptibility χ_v, for materials commonly found in NMR probes. The desired plating thickness for foil is that for which the algebraic sum of the product of thickness and χ_v for the different layers is zero.

4 WIDELINE

The initial instrumentation for solids NMR borrowed extensively from radar and UHF transmitter technology, using fixed-frequency transmission lines as circulators and magic-Ts to isolate the multikilowatt transmitter from the low-noise preamplifier.[2,3] However, it was soon determined that it was not difficult to deal with the phase transients from Qs of 50–200—an order of magnitude higher than initially thought. Pulse rise times could be as much as one-third the pulse length without serious difficulties.[21] Hence, several hundred watts were sufficient except perhaps for low-γ nuclei. The cost savings of moderate power transmitters and the shift from transmission line traps to lumped elements facilitated the commercial solids probe,[22] which is usually required to be multinuclear and reasonably user friendly.

For proton NMR it is still beneficial to damp the Q to about 100 by coating the coil with tin–lead solder (as proton linewidths are large and sensitivity is enormous) but care must be taken not to trap rosin in the coating, or backgrounds will be seen. Also, experiments on other nuclides with very broad lines may benefit from moderate Q-damping if samples larger than 0.1 mL are being used, since the increased bandwidth simplifies data collection. A number of accelerated ringdown schemes have been proposed,[2,23] but the method seeing more use today appears to be overcoupling[24,25] because of noise, reliability, and magnetism problems associated with other methods. Moreover, the recent availability of linear prediction often obviates the need for active damping (see ***Fourier Transform & Linear Prediction Methods***).

The unbalanced, capacitively matched DT circuit (see ***Probe Design & Construction***, Figure 6) is usually used for wideline probes to simplify multinuclear tuning. The HF tuning coil L_H (which may be a capacitively shortened $\lambda/4$ coaxial transmission line) is chosen to have an inductance such that its untuned reactance would be between 25 Ω and 60 Ω at the HF. Lead inductance is minimized subject to VT, high voltage, and multinuclear constraints. The total series lead inductance is then typically 25–40 nH.[14] Maximum B_1/V_T, where V_T is the maximum total circuit voltage, is obtained for coil inductance L_S half of the total circuit inductance, but a somewhat higher value is usually selected for improved LF sensitivity with some sacrifice in HF efficiency and a slight reduction in maximum B_1.

Minimum 90° pulse lengths have typically been 3 μs, but recent successful demonstrations of wideline ^{2}H Hadamard NMR[26] may have a major impact on single resonance solids NMR. In Hadamard NMR, the spin system response to the application of a large number of pseudorandom pulses with flip angles as small as 0.1° (mW, μs pulses) at periods on the order of tens of microseconds can be transformed into the equivalent NMR response from a single high-power pulse. A Hadamard wideline probe should benefit from a low-Q (~5) saddle excitation coil in combination with a moderate-Q (~100) solenoid receive coil. SNR for Hadamard appears comparable to Fourier transform (FT). (See also ***Stochastic Excitation***.)

5 MAGIC ANGLE SPINNING

In 1958, Raymond Andrew[27] and co-workers showed that high-speed sample spinning at the 'magic' angle of 54.7° could be an effective tool in averaging out dipolar broadening. However, the required rotational rates for abundant dipolar nuclei (35 kHz for ^{1}H) appeared impossible, and the technique was largely ignored[28] for nearly two decades until Stejskal and Schaefer[4,5] showed that more realistic rotational rates (3–5 kHz), capable of averaging chemical shift anisotropy, combined with high-power decoupling to remove the ^{1}H dipolar broadening, could be extremely effective in obtaining high-resolution ^{13}C spectra from solid samples.

Andrew used a conical bearing/drive surface which eventually achieved speeds in excess of 10 kHz using helium gas.[29] This spinner was based on the classic ultracentrifuge work by Beams[30] and depended on the Bernoulli effect to hold the sample spinner close to the drive jets. The stiffness of such a bearing is extremely low, which results in low-frequency oscillations, precession, and instabilities. Moreover, angular accuracy of 0.3° is sometimes required in MAS, which is an order of magnitude beyond the capability of the conical Bernoulli–Beams bearing. Lippmaa,[31] Veeman, Pines, Eckman, and others introduced the double bearing cylindrical rotor to circumvent these problems, and Doty and Ellis presented an approximate analysis of the cylindrical air bearing optimization.[32] [Note that typographical errors resulted in equations (9) and (12) in the referenced article[32] appearing twice. The second equation in each case is correct. The first should be deleted.]

The high-strength ceramics[8] that have recently become available are required to obtain high sensitivity (from high filling factor) and high spinning speeds simultaneously. Silicon nitride[33] has the highest strength-to-mass ratio of any available ceramic, which allows the highest surface speeds with low-density samples; but zirconia has higher strength, better toughness, and fewer defects, making it the preferred material for heavier samples—except perhaps at very high fields or high temperatures. Most commercial MAS rotors and stators are ground and lapped (using precision diamond tooling) from partially stabilized zirconia (PSZ) or hot isostatic pressed (HIPd) Si_3N_4. As a consequence, these items are rather expensive. The press-fit turbine caps are usually machined from Vespel, as polyether ether ketone (PEEK) has poor wear resistance despite its other desirable properties. Zirconia turbines may be attached to a

For References see p. 4484

zirconia rotor by thermal interference fit. Other high-strength plastics and ceramics as listed in Table 3 are also used for special thermal or background considerations. Fiber-optics spin-rate detection is normally provided to allow precise, synchronous pulsing for the total suppression of sidebands (TOSS) technique.[34]

5.1 High-Speed Air Bearings

The high mass of ceramic rotors requires more attention to rotor resonances than was required in the earlier designs using plastic rotors.[35] For stability throughout a wide speed range, it is advantageous to have the high bearing stiffness that comes from tight radial clearances. However, as the clearance is reduced, bearing frictional heating becomes more severe; moreover, the possibility of a 'crash' increases. A crash may occur in a hydrostatic bearing when the rotor moves close enough to the stator to cause extreme choking around the perimeter of the bearing nozzles on the proximal side, at which point the stiffness changes sign and the rotor is driven into the stator. Pockets or recesses at the orifice exit may eliminate this crash mechanism,[36] but the reduced response time adversely affects stability at very high speeds unless the pockets are very small.[37]

Highest spinning speeds have been obtained with the design illustrated in Figure 2, which has achieved surface speeds in excess of the speed of sound at room temperature for rotor diameters from 5–14 mm. Half of the bearing gas exits over the ends of the rotor forming an axial thrust bearing at each end, while half exits out the center of the stator. Allowing the gas to flow axially inward as well as outward (nearly) doubles the bearing stiffness (by nearly doubling effective area) and was probably the most significant innovation in the spinner by Langer et al.[38] which achieved a 40% increase in surface speed over previous designs.

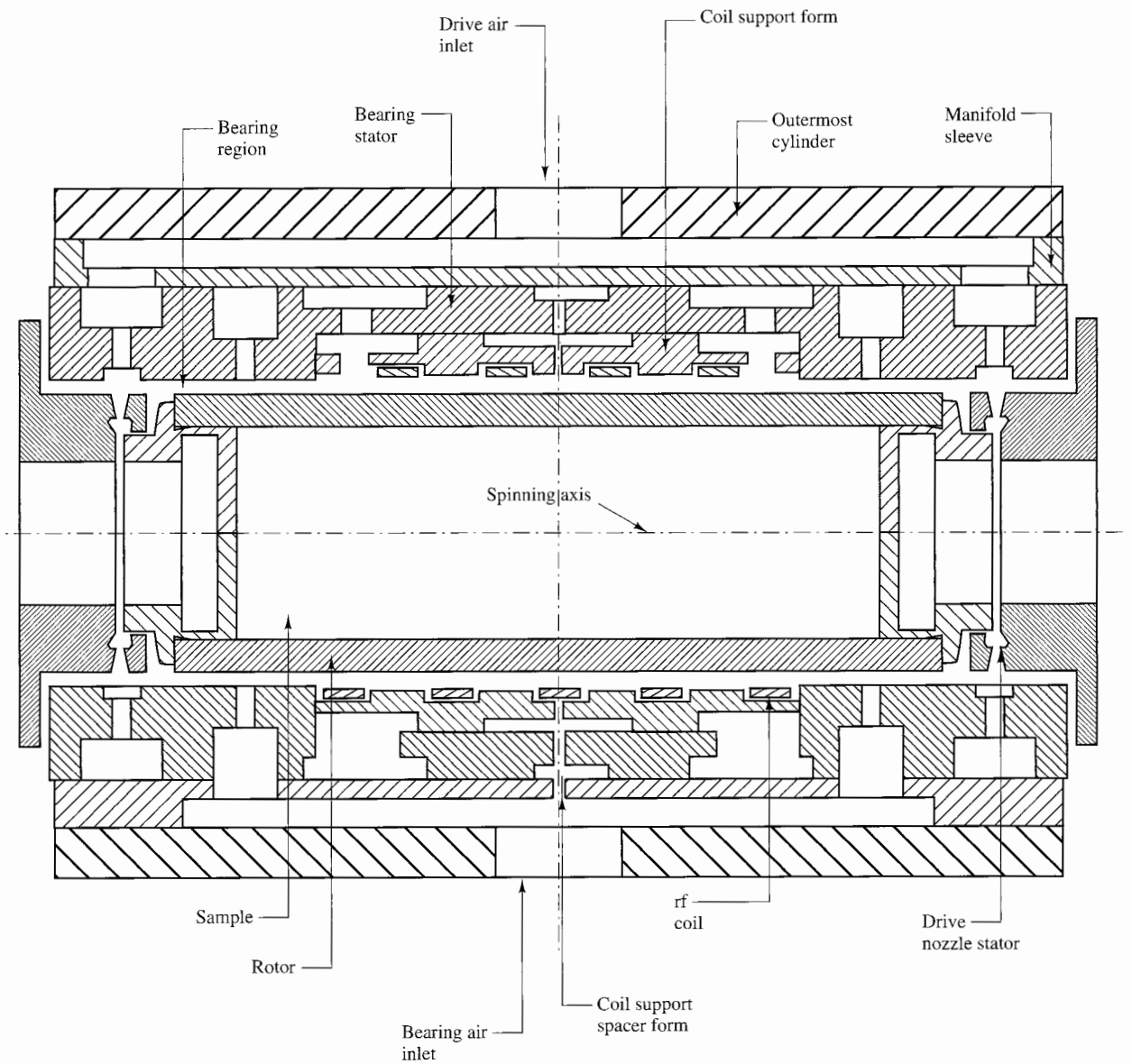

Figure 2 Supersonic sample spinner (Doty Scientific, Inc.)

For list of General Abbreviations see end-papers

Optimum bearing radial clearance for controlling Taylor vortices[39] in the air bearing at moderate speeds is proportional to $(\mu^2 d/c^2\rho^2)^{\frac{1}{3}}$, where μ is the gas viscosity, d is the rotor diameter, c is the velocity of sound, and ρ is the gas density. Optimum clearance r_c for the control of whirl instabilities with minimum friction at high speeds fits the following empirical equation for typical NMR spinners:

$$r_c \cong kT^{-0.25}d^{0.4} \text{ (mixed units)} \quad (1)$$

where T is the gas temperature (K), d is the rotor diameter in mm, and k has an approximate numerical value of 0.0027 for nitrogen and 0.0035 for helium with units of $K^{-0.25}$ $mm^{0.6}$; it is necessary to take into account the strain that will occur even in ceramic rotors at top speeds: 0.1% and 0.15% for silicon nitride and zirconia, respectively. Smaller clearances than given by equation (1) may be used if the additional heating can be tolerated, and larger clearances may be used with large rotors if other measures are taken to control whirl instabilities. Optimum bearing hole size is such that bearing mass flow at 0.3 MPa with the rotor in place is 60%–85% of the mass flow with the rotor removed. Short bearing hole sizes normally range from 0.13 mm for 3.5-mm rotors to 0.28 mm for 14-mm rotors, but slightly larger long bearing holes work better for VT.

With very small rotors, the bearing clearance becomes extremely critical—partly for manufacturing reasons and partly for fundamental reasons. To appreciate the fundamental limitation, consider the conical resonance frequency,[32] which is approximately proportional to the square root of the quotient of the bearing stiffness and the rotor mass near the end of the rotor. In order for this resonance to scale as $1/d$, the stiffness must be linear with diameter (since the mass is cubic with diameter), which requires the radial clearance to be proportional to the diameter if the pressure is constant. But clearance cannot be linear with diameter or frictional power density on the rotor surface becomes unmanageable with small rotors. Hence, Nature does not like small rotors, and it is in fact fortuitous that 5-mm rotors can achieve supersonic surface speeds (21 kHz) under optimum conditions with nitrogen bearing pressures of 0.5 MPa. While 3.5-mm Si_3N_4 rotors have occasionally reached 27 kHz, they are fraught with instabilities above 24 kHz which are exacerbated by the large, axial Bernoulli effects from poor turbine efficiency.

5.2 Radial-Inflow Microturbines

To achieve surface speeds above 240 $m\,s^{-1}$ it is necessary to use microturbines in a symmetrical fashion so that axial reaction forces are precisely balanced at all speeds (unless helium drive gas is used), since the load capacity of the axial thrust bearings is quite limited.[40] The reduced-diameter radial-inflow microturbines used in Figure 2 achieve order-of-magnitude higher isentropic efficiency that the earlier Peltier microturbines by (a) controlling flow separation over the blades, (b) operating at lower tip speed, and (c) reducing exhaust swirl.[41] Inlet and exit angles are not particularly critical, but axial clearance over the blades is—unless the turbine is designed for a very low reaction ratio. A vaneless radial-inflow supersonic diffuser may be used with the larger sizes to obtain supersonic, nonseparated flow at the rotor entrance. The microturbines on a 14-mm rotor have 28 blades with 10-mm tip o.d. and produce 25 W shaft power each at 40% isentropic efficiency at 6 kHz. The 2.5-mm o.d. microturbines on the 3.5-mm rotor have only 12 blades and achieve approximately 10% efficiency at 22 kHz. Unlike large turbines, substantial efficiency losses occur in the nozzles (even with the 14-mm spinners) because of boundary layer effects. For an excellent treatment of turbine theory and design, the reader is referred to the text by Wilson.[42]

5.3 Radiofrequency Circuits

Most MAS work requires CP and/or high-power decoupling. Hence, the circuit is essentially identical to that described earlier for the DT wideline probe except that lead inductance may be a little larger,[14] necessitating somewhat higher sample coil inductance for high sensitivity. Maximum $\boldsymbol{B}_1$ is usually 30% less than expected of a similar DT wideline probe, but many wideline experiments are still possible with an MAS probe. For large samples at high fields, it can be beneficial to balance the HF channel for more efficient decoupling—especially at high temperatures. A modified form of the standard ^1H–^2H high-resolution balanced decoupler/lock circuit may be adapted to the high-power requirements of solids.[43]

Wu and Zilm[44] showed that high rf homogeneity is much more important than originally recognized for efficient CP at high speeds and that variable amplitude proton $\boldsymbol{B}_2$ can greatly improve CP efficiency in the presence of large rf inhomogeneity. Leifer[45] recently presented an elegant method of optimizing rf homogeneity for six- and 10-turn solenoids. Many software packages using numerical methods are now available for general field calculations and optimizations, and a few are capable of properly handling nonuniform surface current distributions.[46]

Single resonance circuits can efficiently use very low inductance coils (e.g., two-turn, 6-mm, 18-nH coils) to achieve the short $\pi/2$ pulse lengths (1.5 μs) needed for multiple pulse techniques to average dipolar interactions of abundant ^1H or ^{19}F nuclei.[4] When combined with sample spinning at several kHz to average chemical shift anisotropy, the technique is called combined rotation and multiple pulse spectroscopy (CRAMPS). High resolution in CRAMPS requires extremely high $\boldsymbol{B}_1$ homogeneity. Since wide conductors and leads are required with low-inductance coils (to limit lead voltage, if not losses), the current locations are not known and the method of Leifer and related analytical methods cannot be used to homogenize the field. However, the most difficult technical problem in making CRAMPS probes is usually that of eliminating proton background signals from hydrogenous contaminants in Teflon and even Kel-F.

Triple resonance circuits have been used occasionally for more than a decade,[47] but the development of the powerful rotational echo double resonance (REDOR) technique[48] for accurate distance determinations from weak dipolar couplings has recently resulted in a large demand for triple resonance MAS probes. The circuit shown in Figure 3 uses an inductively coupled HF tank to permit multinuclear tuning at both the middle and the low frequency with high efficiency and excellent isolation on all ports.[49] It has been used successfully for ^1H up to 500 MHz, and can easily be extended to quad resonance experiments such as RETRO.[50] Fixed frequency triple

For References see p. 4484

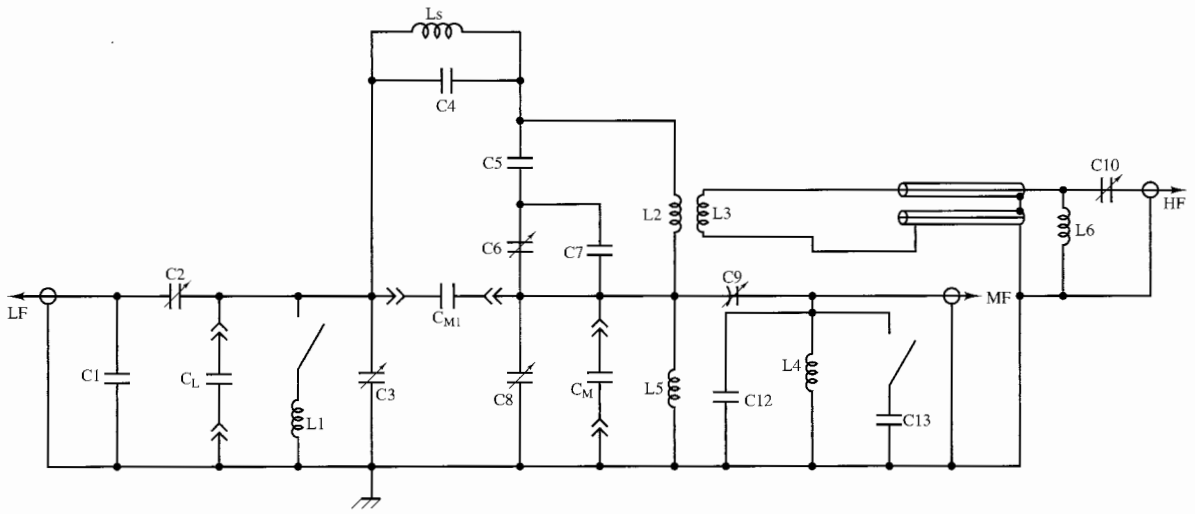

Figure 3 Doubly broadband, triple resonance circuit (Doty Scientific, Inc.)

resonance MAS probes for REDOR experiments are expected to be available soon at 750 MHz.

6 GONIOMETERS AND SLOW MAS

The earliest applications of NMR to solids involved the study of single crystals, as relatively narrow lines are observed without multiple pulse or high-speed spinning techniques. These studies are necessarily limited to materials that can be obtained in single crystals of sufficient size (usually several mm^3) for acceptable S/N. The method requires the ability to slowly and precisely rotate the crystal about three orthogonal axes while observing the anisotropic chemical shift. The standard method for the past two decades has involved gluing a small crystal into a three-sided, 4-mm 'semicube'.[6] (Similar probes with larger coils have rotated sealed tubes to study oriented liquid crystals.) The sample may then be inserted into a precision holder inside the sample coil for 360° rotation about an axis perpendicular to $\boldsymbol{B}_0$ in small increments at which spectra are collected. The semicube is then removed and reinserted for rotation about a second axis, and the process is repeated again for the third axis. The crystal orientation with respect to the semicube holder is determined using X-ray crystallographic techniques.

The sample holder axis may be inclined at the magic angle to permit slow MAS, which is a method of addressing the spinning sideband problem by applying pulses precisely at 0°, 120°, and 240°. There is renewed interest in this technique for obtaining high-resolution spectra from large samples of dilute systems. (See ***Magic Angle Turning & Hopping***.)

Rotation has usually been accomplished using precision aluminum or brass bevel gears, but worm gears, belts, and flexible shafts have also been used. The early versions used a manual goniometer, but a stepper motor under computer control is now common. A DT multi-X circuit is usually used.

7 VARIABLE TEMPERATURE (VT)

Most CP MAS probes operate from −120 °C to +160 °C, but XVT CP MAS probes are available for wider temperature ranges, and several methods[51] have been used to cool the drive gas and circumvent liquefaction problems in pressurized nitrogen. Gay[52] optimized the conventional high-resolution sample tube spinner to obtain rotational rates sufficient for many MAS applications (over 3 kHz for 5-mm tubes) with the advantages of greater independence of the sample temperature and spinning characteristics and the ability to spin long, sealed glass tubes at the magic angle. The MAS design of Bartuska et al.[53] also provides clear separation between the VT and the bearing gas.

One manufacturer (Doty Scientific) uses a low-temperature and a high-temperature CP MAS probe, as pictured in Figure 4 along with a standard CP MAS probe, to cover the range from 35 K to over 900 K. In these probes, the electronics are maintained near room temperature and positioned close to the sample to allow multinuclear tuning without excessive lead losses, although lead inductance is increased by about 30 nH over the standard probes. Another manufacturer (Bruker) offers a gas-levitated, laser-heated wideline probe for experiments to 1200 °C.[54] Attempts to provide CP MAS down to 6 K have proven too difficult for commercial success thus far, but a number of research groups[55,56] have performed wideline NMR experiments in the 0.03–3 K range.

8 DYNAMIC ANGLE SPINNING (DAS)

High-resolution NMR spectra can be obtained from quadrupolar nuclei if the sample spinning axis can be dynamically reoriented such that the time average of the second and fourth spherical harmonic functions vanishes.[7] The dynamic angle spinning (DAS) probe allows the spinning axis to be rapidly changed while spinning the sample at high speeds to accom-

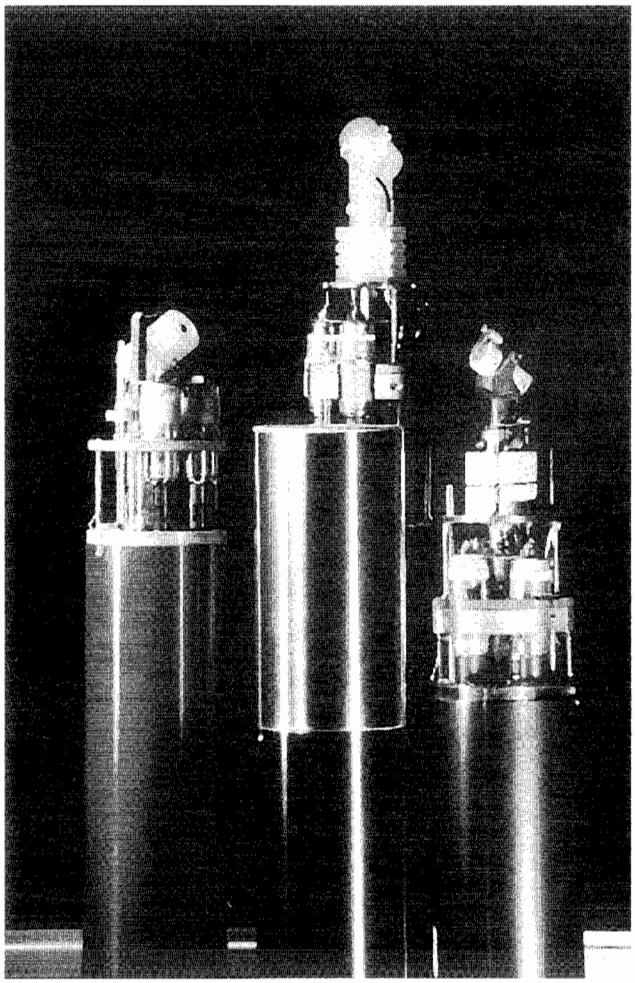

Figure 4 VT CP MAS, low-temperature CP MAS, and high-temperature CP MAS probes

plish the required averaging. One early design used a pneumatic system to switch between two fixed angles, but a high-performance servo motor and precision encoder are now standard, as programming flexibility is needed to experiment with the various 'magic angle pairs' such as [0°, 63.43°], [30.56°, 70.12°], and [37.38°, 79.19°].[57]

Two basic approaches have been used: moving coil and fixed coil. The moving coil design has the rf coil mounted on the spinner stator and attached with flexible leads or sliding contacts.[58] The fixed coil design uses a small spinner assembly that can be rotated perpendicular to its spinning axis inside a large rf coil that is perpendicular to the external field and coaxial with the reorientation axis.[59] The first commercial DAS probes used a moving coil, but it was abandoned in favor of the fixed coil because of lead failures, as most DAS experiments are two-dimensional and require millions of flips. The fixed-coil design has inherently poor filling factor, but special spinners and coils are being developed to minimize this drawback.

High-torque, low-inertia servo motors with optimized linkage should permit axis reorientation under 5 ms if the air bearings supporting the sample rotor have sufficient stiffness and load capacity; but control limitations, linkage compliance, and structure vibrations have often resulted in settling times of 25 ms or more.[59] The currently available commercial DAS probe shown in Figure 5 uses a 21-mm diameter rf coil, 8 mm long, and offers a choice of three interchangeable sample spinners: 8.6-mm diameter by 12 mm; 7-mm diameter by 13 mm;

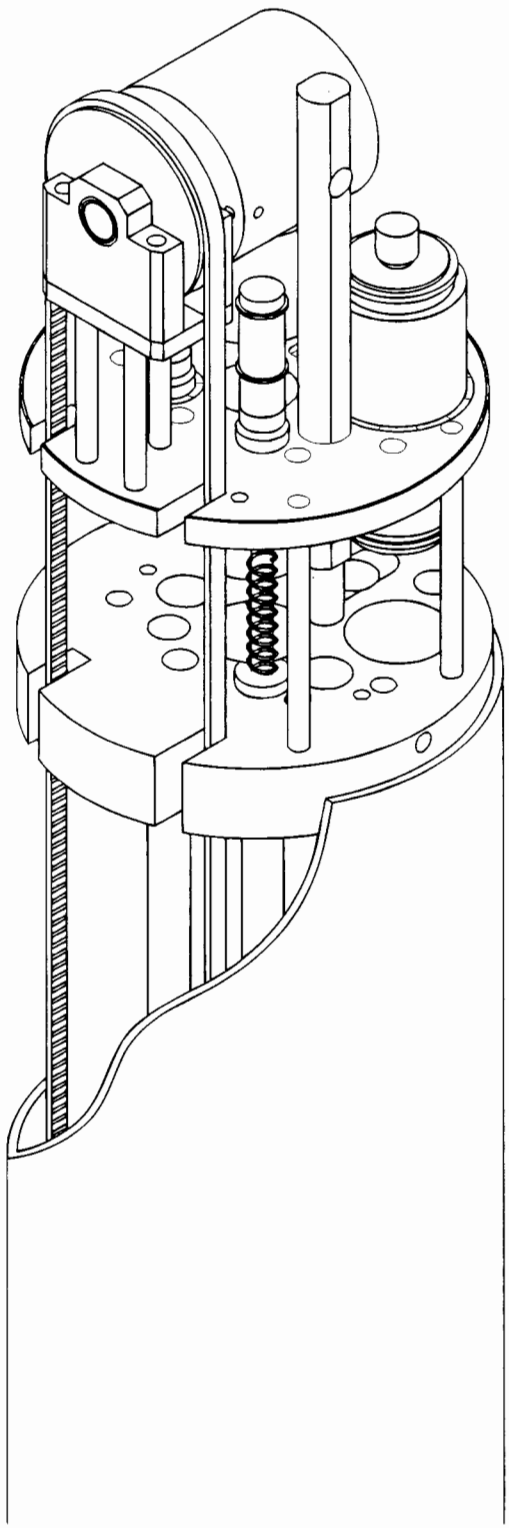

Figure 5 DAS probe with fixed coil and belt-drive spinner reorientation

For References see p. 4484

and 5-mm diameter by 14 mm. The shortest reorientation times thus far with 8.6-mm rotors are about 15 ms. Half that time may be possible with the 5-mm rotors, but the filling factor is very small. One of the factors contributing to the engineering difficulties is that the motor must be positioned well below the magnet to operate properly, which requires a rather long drive linkage that still must allow easy insertion of the probe into the magnet. The other major technical problem is that rotors with small aspect ratio (length-to-diameter ratio) are required for good filling factor, but a large aspect ratio is needed for bearing stability during rapid reorientation.

9 DOUBLE ROTATION (DOR)

In the DOR technique, the sample is placed in a small spinner inside a larger spinner and spun about two intersecting axes simultaneously to accomplish the time averaging needed to remove dipolar and quadrupolar interactions. It usually comes as a surprise to the uninitiated that such a feat would be possible at high speeds, even though most have observed a football traveling through the air executing free precession—spinning about two axes simultaneously with no significant external torques acting upon it.

The requirement for no net torques on the inner rotor is given by the following:

$$f_1 = \frac{f_2(I_T - I_A)\cos\theta_2}{I_A} \quad (2)$$

where f_1 is the frequency of the inner rotor, f_2 the frequency of the outer rotor, I_A the *axial* moment of inertia of the inner spinner (rotor, sample, caps), I_T the *transverse* moment of inertia of the inner spinner, and θ_2 is the angle of the inner rotor with respect to the axis of the outer rotor.[60]

In practice, the outer rotor is always inclined at the dipolar magic angle, 54.7°, and θ_2 is 30.56°. For stability, (a) f_1 must be a few per cent larger than given by the above, (b) the center of mass of the inner rotor must lie precisely on the axis of the outer rotor, and (c) the outer rotor must be dynamically balanced when the inner rotor is removed. The highest double rotation rates thus far are approximately 1800 Hz outer and 7000 Hz inner for 0.1-mL samples. The outer spinner assembly of a DOR spinner is shown in Figure 1, inclined at 54.7°. (The braid-reinforced lines entering each end of the assembly supply air to the inner spinner.)

10 RELATED ARTICLES

Ceramics Imaging; CRAMPS; Double Rotation; Dynamic Angle Spinning; Magic Angle Spinning; Probe Design & Construction; Probes for Special Purposes.

11 REFERENCES

1. S. R. Hartmann and E. L. Hahn, *Phys. Rev.*, 1962, **128**, 2042.
2. P. Mansfield and J. G. Powles, *J. Sci. Instrum.*, 1963, **40**, 232.
3. J. S. Waugh, *US Pat. 3 530 373*, 1970.
4. R. W. Vaughan, *Annu. Rev. Phys. Chem.*, 1978, **29**, 397.
5. E. O. Stejskal, J. Schaefer, and J. S. Waugh, *J. Magn. Reson.*, 1977, **28**, 105.
6. R. S. Honkonen, F. D. Doty, and P. D. Ellis, *J. Am. Chem. Soc.*, 1983, **105**, 4163.
7. B. F. Chmelka and A. Pines, *Science*, 1989, **246**, 71.
8. S. J. Schneider (ed.), 'Engineered Materials Handbook', Vol. 4, 'Ceramics and Glasses', ASM International, Novelty, OH, 1991.
9. R. C. Buchanan (ed.), 'Ceramic Materials for Electronics', Marcel Dekker, New York, 1991.
10. J. Agranoff (ed.), 'Modern Plastics Encyclopedia', McGraw-Hill, New York, 1982.
11. J. J. O'Dwyer, 'The Theory of Electrical Conduction and Breakdown in Solids Dielectrics', Oxford University Press (Clarendon), London/New York, 1973.
12. D. R. Lide (ed.), 'CRC Handbook of Chemistry and Physics', 73rd edn., CRC Press, Boca Raton, FL, 1992.
13. J. D. Swift, in 'The Encyclopedia of Physics', 2nd edn., ed. R. M. Besancon, Van Nostrand Reinhold, New York, 1974, pp. 249–253.
14. F. D. Doty, T. J. Connick, X. Z. Ni, and M. N. Clingan, *J. Magn. Reson.*, 1988, **77**, 536.
15. S. L. Patt, *US Pat. 4 438 400*, 1984.
16. D. G. Hughes and L. Pandey, *J. Magn. Reson.*, 1984, **56**, 428.
17. M. L. Buess and G. L. Petersen, *Rev. Sci. Instrum.*, 1978, **49**, 1151.
18. F. D. Doty, *US Pat. 4 710 719*, 1987.
19. D. I. Hoult and R. E. Richards, *J. Magn. Reson.*, 1976, **24**, 71.
20. D. I. Hoult, *Prog. Nucl. Magn. Reson., Spectrosc.*, 1978, **12**, 41.
21. R. W. Vaughan, D. D. Elleman, L. M. Stacey, W. K. Rhim, and J. W. Lee, *Rev. Sci. Instrum.*, 1972, **43**, 1356.
22. F. D. Doty, R. R. Inners, and P. D. Ellis, *J. Magn. Reson.*, 1981, **43**, 399.
23. W. G. Clark and J. A. McNeil, *Rev. Sci. Instrum.*, 1973, **44**, 844.
24. G. C. Chingas, *J. Magn. Reson.*, 1983, **54**, 153.
25. D. I. Hoult, *J. Magn. Reson.*, 1984, **57**, 394.
26. M. Greferath, B. Blumich, W. M. Griffith, and G. L. Hoatson, *J. Magn. Reson., Ser. A*, 1993, **102**, 73.
27. E. R. Andrew, A. Bradbury, and R. G. Eades, *Nature (London)*, 1958, **182**, 1659.
28. J. D. Ellett, M. G. Gibby, U. Haeberlen, L. M. Huber, M. Mehring, A. Pines, and J. S. Waugh, in 'Advances in Magnetic Resonance', ed. J. S. Waugh, Academic Press, New York, 1971, Vol. 5, pp. 117–176.
29. E. Andrew, L Farnell, M. Firth, T. Gladhill, and I. Roberts, *J. Magn. Reson.*, 1969, **1**, 27.
30. J. W. Beams, *J. Appl. Phys.*, 1937, **8**, 795.
31. E. T. Lippmaa, M. A. Alla, A. A. Salumyae, and T. A. Tukherm, *US Pat. 4 254 373*, 1981.
32. F. D. Doty and P. D. Ellis, *Rev. Sci. Instrum.*, 1981, **52**, 1868.
33. J. Adlerborn, M. Burstrom, L. Hermansson, and H. T. Larker, *Mater. Design*, 1987, **8**, 229.
34. W. T. Dixon, J. Schaefer, M. D. Sefcik, E. O. Stejskal, and R. A. McKay, *J. Magn. Reson.*, 1982, **49**, 341.
35. V. J. Bartuska and G. E. Maciel, *J. Magn. Reson.*, 1981, **42**, 312.
36. W. B. Rowe, 'Hydrostatic and Hybrid Bearing Design', Butterworths, London, 1983.
37. F. D. Doty, *US Pat. 4 456 882*, 1984.
38. V. Langer, P. Daugaard, and H. J. Jakobsen, *J. Magn. Reson.*, 1986, **70**, 472
39. D. Dowson (ed.), 'Superlaminar Flow in Bearings', MEP, London, 1975.
40. F. D. Doty, J. B. Spitzmesser, and D. G. Wilson, *US Pat. 5 202 633*, 1993.
41. F. D. Doty, B. L. Miller, G. S. Hosford, D. G. Wilson, W. Huanbo, and J. D. Jones, 'Proc. IECEC-91', 1991, Vol. 2, SAE, Warrendale, PA, p. 436.

For list of General Abbreviations see end-papers

42. D. G. Wilson, 'The Design of High-Efficiency Turbomachinery and Gas Turbines', MIT Press, Cambridge, 1984.
43. F. D. Doty, *US Pat. 5 162 739*, 1992.
44. X. Wu and K. Zilm, *J. Magn. Reson., Ser. A*, 1993, **104**, 154.
45. M. C. Leifer, *J. Magn. Reson., Ser. A*, 1993, **105**, 1.
46. G. J. Kost, S. E. Anderson, G. B. Matson, and C. B. Conboy, *J. Magn. Reson.*, 1989, **82**, 238.
47. S. Kan, M. Fan, and J. Courtieu, *Rev. Sci. Instrum.*, 1980, **51**, 887.
48. T. Gullion and J. Schaefer, in 'Advances in Magnetic Resonance', ed. W. S. Warren, Academic Press, San Diego, CA, 1989, Vol. 13, pp. 57–83.
49. F. D. Doty, 'Doubly Broadband Triple Resonance Circuit', *US Pat. 5 424 645*, 1995.
50. S. M. Holl, R. A. McKay, T. Gullion, and J. Schaefer, *J. Magn. Reson.*, 1990, **89**, 620.
51. R. D. Kendrick, S. Friedrich, B. Wehrle, H. H. Limbach, and C. S. Yannoni, *J. Magn. Reson.*, 1985, **65**, 159.
52. I. D. Gay, *J. Magn. Reson.*, 1984, **58**, 413.
53. V. J. Bartuska, D. H. Lewis, R. B. Lewis, and D. G. Dalbow, *US Pat. 4 511 841*, 1985.
54. D. Massiot, C. Bessada, P. Exchegut, J. P. Coutures, and F. Taulelle, *Solid State Ionics*, 1990, **37**, 223.
55. K. Carduner, M. Villa, and D. White, *Rev. Sci. Instrum.*, 1984, **55**, 68.
56. J. L. Weil, S. L. Tan, J. S. Waugh, and D. D. Osheroff, *J. Magn. Reson.*, 1987, **66**, 264.
57. B. Q. Sun, J. H. Baltisberger, Y. Wu, A. Samoson, and A. Pines, *Solid State NMR*, 1992, **1**, 267.
58. K. T. Mueller, B. Q. Sun, G. C. Chingas, J. W. Zwanziger, T. Terao, and A. Pines, *J. Magn. Reson.*, 1990, **86**, 470.
59. K. T. Mueller, G. C. Chingas, and A. Pines, *Rev. Sci. Instrum.*, 1991, **62**, 1445.
60. Y. Wu, B. Q. Sun, A. Pines, A. Samoson, and E. Lippmaa, *J. Magn. Reson.*, 1990, **89**, 297.

Biographical Sketch

F. David Doty. *b* 1950. B.A., 1972, physics, Anderson University, IN, USA, Ph.D., 1983, Physics, University of South Carolina. Began work in NMR under Paul Ellis, 1979. President of Doty Scientific, Inc., 1982–present. Approx. 20 publications and 15 patents. Research interests include rf electronics, NMR probe technology, electromagnetism, manufacturing, turbomachinery, energy conversion cycles, ceramics engineering, acoustics, economics, and religions.

Sonicated Membrane Vesicles

Wen-guey Wu

National Tsing Hua University, Hsinchu, Taiwan

1 INTRODUCTION

Current understanding of the structure and dynamics of lipids in membranes is, to a large extent, promoted by the availability of various membrane model systems. Sonicated membrane vesicles, or small unilamellar vesicles first characterized and prepared by Huang in 1969, have been utilized extensively in NMR studies because of the high-resolution features in their spectra. A reflection on how the original idea was conceived to prepare a homogeneous fraction of a sonicated membrane vesicle is given by C. Huang.[1] Much structural and dynamic information of membrane lipids was thus inferred before the advent of solid state NMR spectroscopy suitable for unsonicated membrane studies. Therefore, solution NMR studies of sonicated membrane vesicles may be considered to have played a pioneering role for the solid state NMR investigation of planar membranes.

The interest in studying sonicated membrane vesicles, however, extends beyond a simple model membrane system for NMR studies. There is a growing interest in how curvature of the lipid/water interface affects packing of the lipid acyl chains.[2,3] It has been suggested that the curved membrane surface may be important in affecting protein–lipid interactions. The discussions and endeavors for settling the controversial issue in the interpretation of fatty acyl chain order derived from NMR studies of small vesicles in comparison to planar membranes has also attracted many ingenious NMR approaches. Progress in the application of NMR lineshape analysis to studies of the molecular ordering and conformations of membrane lipids and in the interpretation of nuclear spin relaxation experiments has been made possible partially because of these efforts.

One of the important criteria for the quantitative interpretation of the NMR spectra of sonicated membrane vesicles, unfortunately often neglected, is the homogeneity of the spin systems used for experiments.

First, simple sonication of aqueous dispersions of phospholipids does not produce the homogeneous preparation of

For References see p. 4491